Geologic setting and seismic surveys

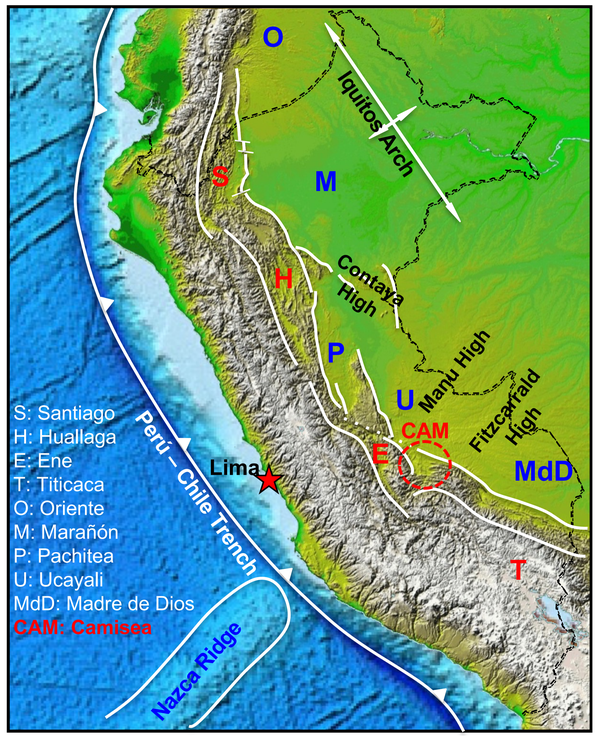

Figure 1: Location of the study area relative to the west coast of South America, in the foothills of the Peruvian Andes

Geologic setting

Area located 450 km from Lima, in southern Ucayali Basin (Figure 1).

Stratigraphy: 8000+ m Paleozoic, Mesozoic and Cenozoic sedimentary rocks (Figure 2).

Tectonic domains in the area:

- Thick-skin fold and thrust belt (FTB)
- Thin-skin FTB
- Foreland basin

3D surveys of 1250 km², mostly over thin-skin FTB, extending partially into neighbouring domains (Figure 3).

Hydrocarbon traps in regional, 100+ km long fault-bend folds with clear surface expression (Figure 4)

- Lower detachment level: Cabanillas Gr (Devonian)
- Upper detachment level: base of Tertiary "Red Beds"
- A single frontal backthrust releases most of the slip (Figure 2)
- Shortening of more than 23 km, 2000+ m structural relief
- Camisea Supergiant holds 25 TCF gas + condensate recoverable resources from 5 main reservoirs

The area is described in further detail by Boyer and Elliot (1982), DeCelles (1996), Disalvo et al (2022), McClay et al (2018) and Zamora et al (2019), among others.

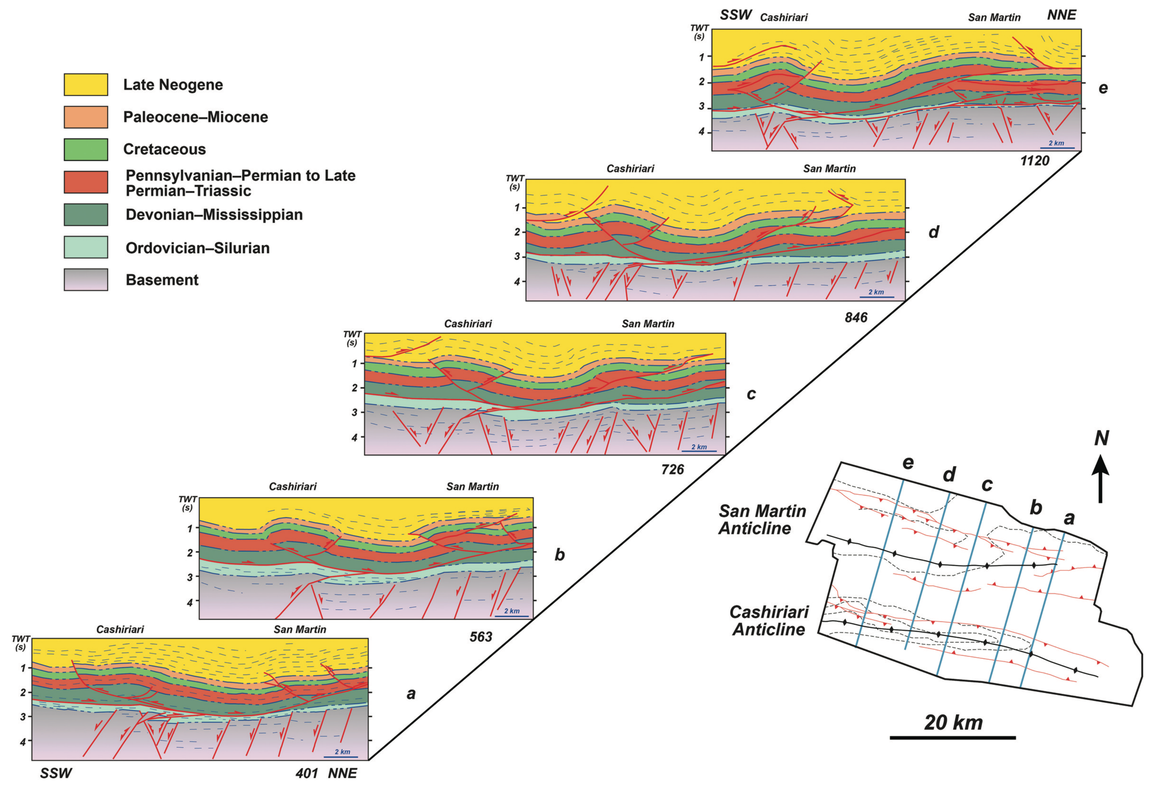

Figure 2: Structural cross-sections from the Camisea 3D, at the east end of the 3D merged area from McClay et al. (2018).

Seismic surveys

There are three seismic surveys included in the seismic-imaging project (Figure 3). The Camisea 3D was the original survey, shot in 2002. Then the Pagoreni survey was shot in 2005 extending coverage to the west. The source and receiver lines followed the same azimuth, but the source line interval decreased, reducing the density of coverage. There was a small overlap area between the surveys, but, in spite of the small overlap, minimal technical problems were found when merging the volumes.

Pagoreni was shot in two phases. There was little interest in the western side of the Pagoreni survey, and, instead of filling the gap with 2D seismic lines, the consortium decided to acquire a half-fold 3D seismic survey. The half-fold area can be seen on the west end of the Pagoreni survey in Figure 3. The extension of the 3D coverage continued in 2009 with the Mipaya survey.

The geologic map in Figure 4 shows the outline of the surveys and a grid of inlines from the 3D. The main anticlinal structures have clear surface expressions.

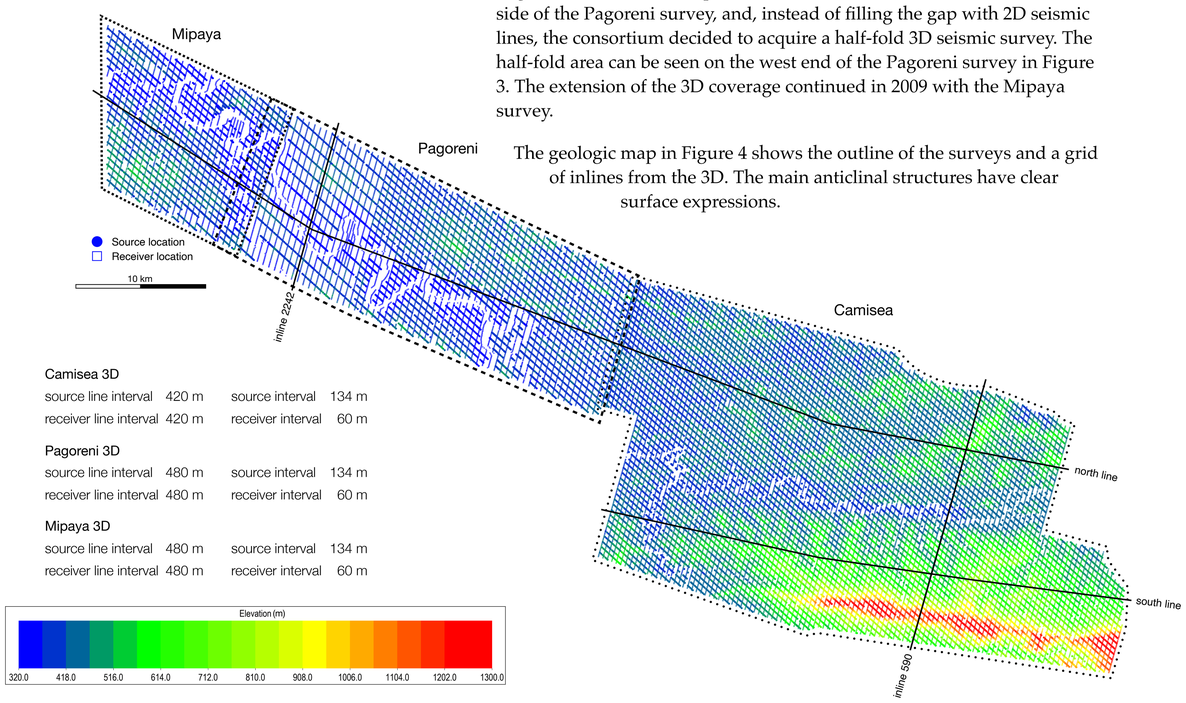

Figure 3: Seismic coverage map of the source and receiver lines for the three 3D surveys: Camisea, Pagoreni, and Mipaya. There are two inlines and two arbitrary lines marked on the figure that are used to illustrate well ties (Figure 7) and compare the final results (Figure 9).

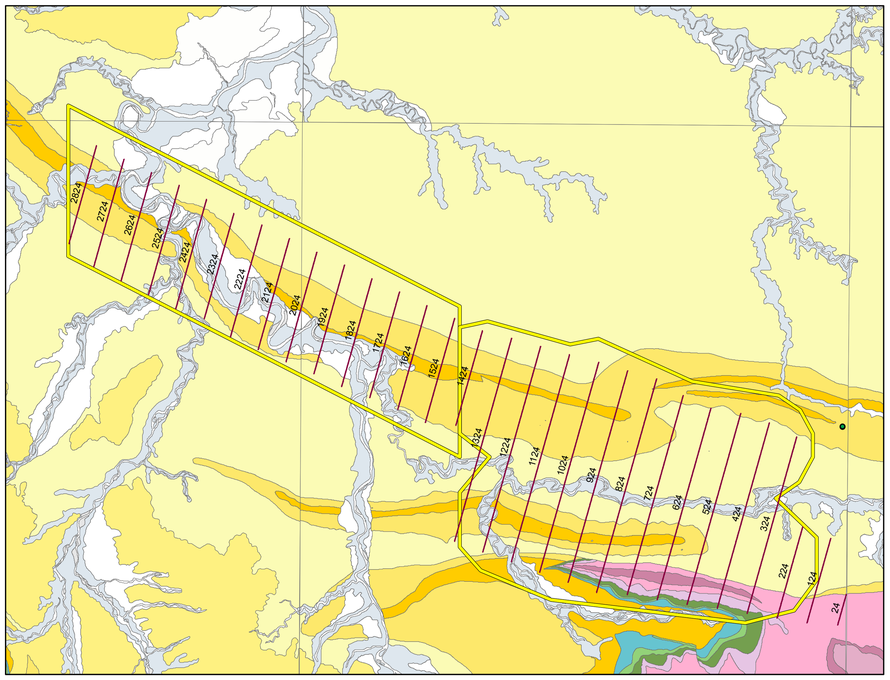

Figure 4: Geologic map with a sequence of 3D inlines overlaid. Note the surface expressions of the main anticlinal and overthrust features.

Geologically constrained model building for seismic depth imaging in Camisea, Perú

Rob Vestrum[1] Juan Soldo[2] Emilse Zunino[2]
María Emilia Muzzio[2] Juan Chung[2]

[1]Thrust Belt Imaging [2]Pluspetrol

Abstract

- Integrated seismic case study from the Peruvian Andes
- Geologic constraints are essential to seismic imaging in complex-structure land areas
  - Surface geology
  - Well logs
  - Structural cross-sections
  - Dip/strike geometry volumes for TTI anisotropic depth migration
- Seismic reflectors on the final depth image closely matched well depths across the block without vertical scaling or calibration
- Revised volume redefined the structural model and revealed an additional subthrust target

Introduction

Difficulties with land seismic data in structured areas:

- Low data density
- Low signal-to-noise ratios
- High geologic complexity

The subsurface velocity model is highly underconstrained by the seismic data, so automated methods for deriving the subsurface velocities required for seismic imaging are highly unstable. We use a workflow similar to Murphy and Gray's (1999) manual-tomography method to leverage the experience of the processor, interpreter, and geologist to overcome these limitations.

Geologic constraints are required to optimize the seismic image.

Model-building method for PSDM

The strategy to overcome the limitations of seismic data in this complex-structured land environment was to integrate geologic constraints into our model-building workflow. The structural geologist provided horizons and faults to constrain the major velocity boundaries. Previous PSDM work in this area and velocities from wells gave us an initial velocity profile to apply to the structural interpretation of the velocity boundaries.

We relied on seismic diagnostics to guide subsequent model-update iterations (Figure 5). Observations from image-gather analysis provided clues as to which rock units needed higher or lower velocity to further optimize the image. Any changes to the velocity model needed to stand up to the test: does this change to the model make geologic sense? Then we tested geologic scenarios and assessed the seismic response.

Well ties further constrained our velocity model. Seismic anisotropy is a major factor in the depth errors on seismic reflectors as compared to well tops, so we corrected for TTI anisotropy throughout our workflow. We expected the seismic reflector depth to match the correlated well top.

What about the dip?

Extensive folding resulted in dipping clastic strata throughout, so it was important to correct for TTI anisotropy in seismic imaging. The velocity model then required two dip volumes: the apparent dip along (1) inline and (2) crossline directions. We investigated using stack coherency to calculate dip volumes, but in the shallow section and in areas of steep dips, the stack coherency was too low for the task. The required dip volumes were interpolated from the horizon geometry from the structural interpretation.

Figure 6 shows a seismic inline with overlays of the two methods for dip calculation: (a) the inline apparent dip calculated from the coherency of the seismic reflectors and (b) shows the inline apparent dip calculated from the horizon geometry. Calculating the dip from the seismic reflectors shows more detail than the dip calculated from the horizons, but, in areas of steep dips, as circled on Figure 6, the coherency method breaks down and calculating dips from the horizon interpretation provides a more accurate dip interpretation. Also, in the shallow section section where coherency is reduced due to decreased data density, the dip trends through the syncline are lost using the coherency method (Figure 6a), and the near-surface is important for depth imaging because it is the lens through which we image the subsurface. We used the interpreted model in this case.

Converging to an optimized velocity model

As we iterated through the model-building process, each model update and model scenario test was based on feedback from previous model iterations. Flatness of the prestack image gather is the primary seismic diagnostic, and we also evaluated changes in stack coherency and geological validity of the reflector geometry. The final test of reflector geometry was the tie between the depths of well tops and the depths of seismic reflectors.

As we iterate through the different model scenarios, we assessed seismic response:

- Have we optimized the seismic imaging?
- Are there imaging improvements compared to the time migration?
- Do the depths of seismic reflectors tie the well depths?

Early in the process, the answers were "no" for much of the volume. We iterated until we could say "yes" to most or all of these questions. Resulting model examples are shown in Figures 5 & 7.

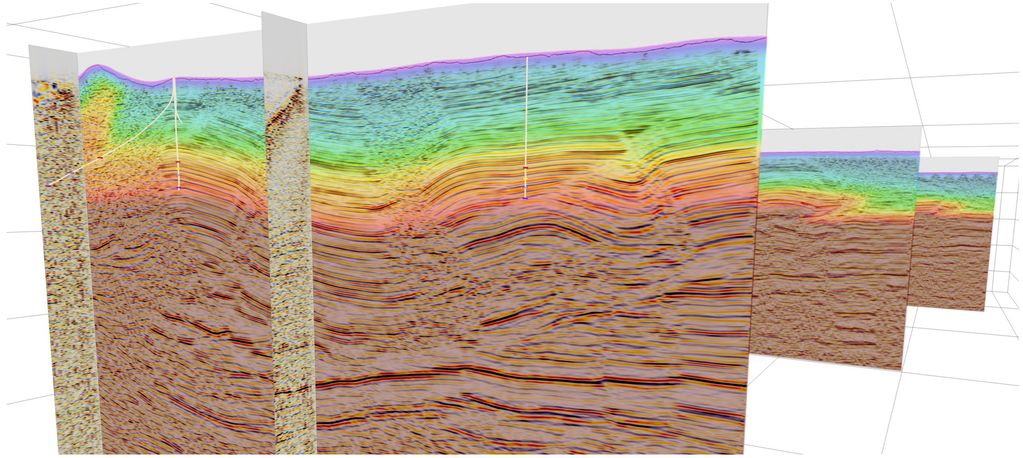

Figure 5: Velocity model overlaid on seismic inline 590 (Figure 3). Image gathers are displayed orthogonal to the inline, with offset increasing outward from the seismic slice. Note the low signal coherency on the image gathers as compared to the stack image.

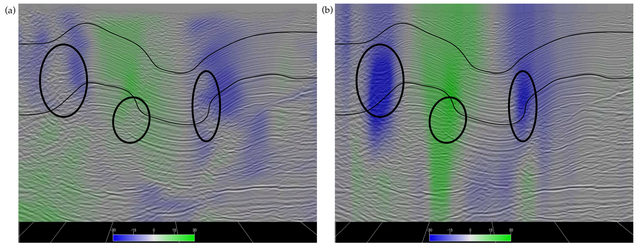

Figure 6: 3D inline slice with apparent dip overlays using two different methods: (a) coherency of the seismic reflectors and (b) interpolated from the horizon geometry. The seismic image is the same between (a) and (b), with the two different methods for dip calculation overlaid. The coherency method (a) shows more detail, but it can miss some of the steeper dips that where the coherency is reduced, as shown in the shallow section and the steep dips circled in black.

Tying wells to seismic

There were 19 wells across the structures (Figure 8). As we began to converge to a velocity model that optimized the seismic imaging, we used the ties between well depths and seismic reflector depths to assess the accuracy of the different velocity-model scenarios that we tested. The depth-migration algorithm corrects for the effects of seismic velocity anisotropy, so we expect the seismic reflector depths to match the depth of the correlated well top. Any differences in depth between seismic reflector and well top are then assumed to result from errors in the depth-migration velocity model.

Once we had a velocity model that resulted in optimized imaging and well-ties within a seismic wavelength, we applied a final tweak to the velocity model to optimize the well ties to within ¼ wavelength. Figure 7 shows a 3D line across five wells along the crest of the Cashiriari structure, before (Figure 7a) and after (Figure 7b) the final velocity update. The two wells along the west plunge of the structure showed seismic reflectors that are low relative to the correlated well top. On the east end, we had the opposite situation, where the seismic reflector was too high. We calculated percentage depth errors and applied those ratios to the velocity model. The colour map shows subtle changes in model velocity (Figure 7), and the seismic coherency is similar, but after the velocity change was applied to the velocity model (Figure 7b), the final migrated image tied the well tops in depth without further depth scaling.

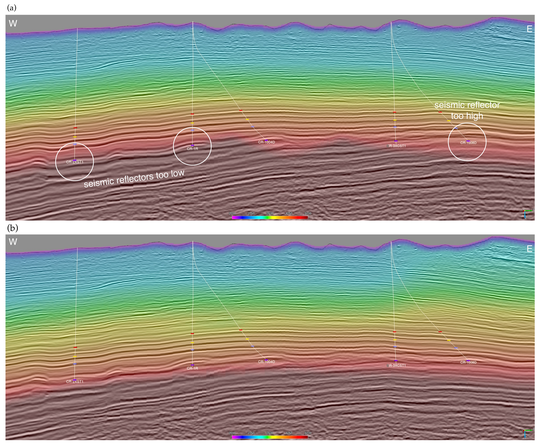

Figure 7: South line (Figure 3) from the 3D along the approximate strike of the Cashiriari structure, connecting the five wells across the structure. The velocity model overlay and its resulting PSDM stack image are shown (a) before and (b) after the final well-tie update of the migration velocity model.

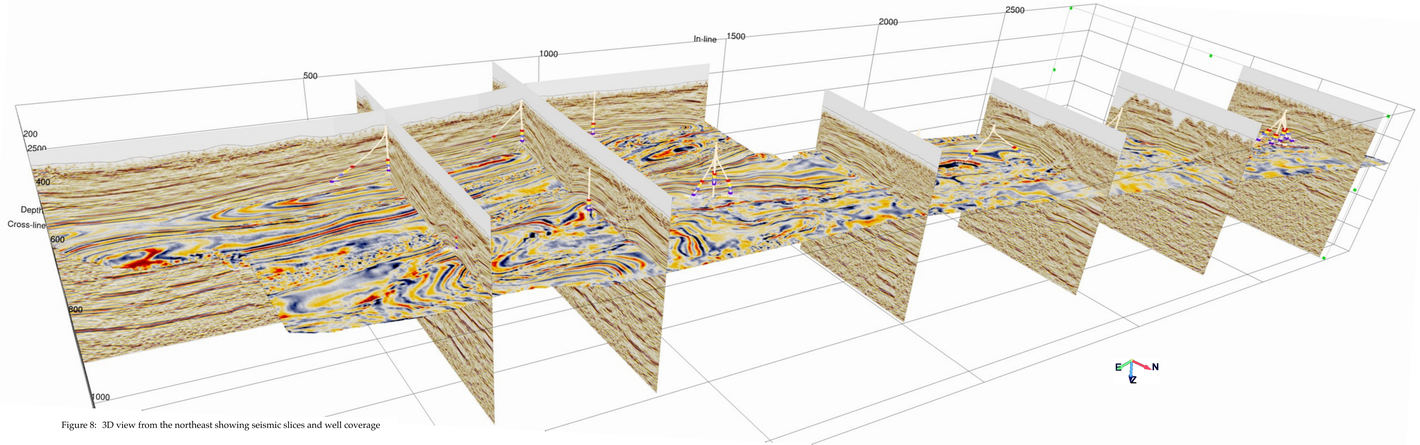

Figure 8: 3D view from the northeast showing seismic slices and well coverage

Results and conclusions

Seismic imaging results

The final volume shows improved detail in the imaging, particularly in the subthrust areas, which are more affected by the cumulative effects of seismic velocity heterogeneity and anisotropy.

The first comparison to the legacy processing is shown in Figures 9a and 9b. This line across the Camisea 3D covers both south and north structures and has wells on each of these. Rectangles on these displays indicate areas of imaging improvement in structural shape and reflector coherency.

The second comparison (Figure 9c and 9d) shows a random line that runs the full east-west extent of the survey, as shown in Figure 3. The differences in imaging are subtle along the crest of this northern structure, but the well tops tie better.

Inline 2242 is in the west region of the survey, in the area of lowest shot density. Figure 9f shows the imaging result as compared to the legacy version (Figure 9e). This area shows the most dramatic improvement over the legacy version. The lower data density, as shown in Figure 3, likely caused instabilities in the automated reflection-tomography method used in the legacy processing (Figure 9e). The geologically constrained velocity model carries the velocity structure through this low-density area, following the interpreted fault geometry and stratigraphic boundaries constrained by well tops. The seismic image shows strong improvement in the foreland on the northern third of this line (Figure 9f).

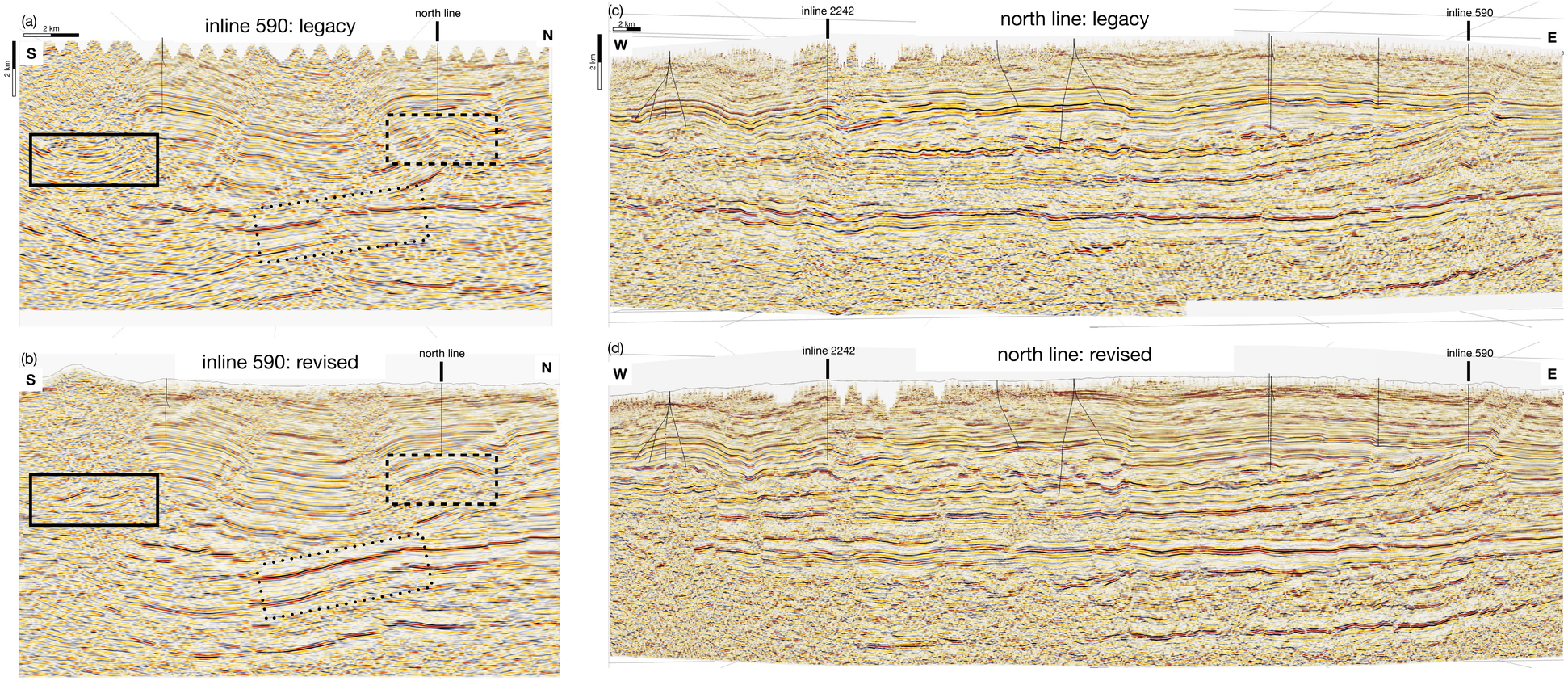

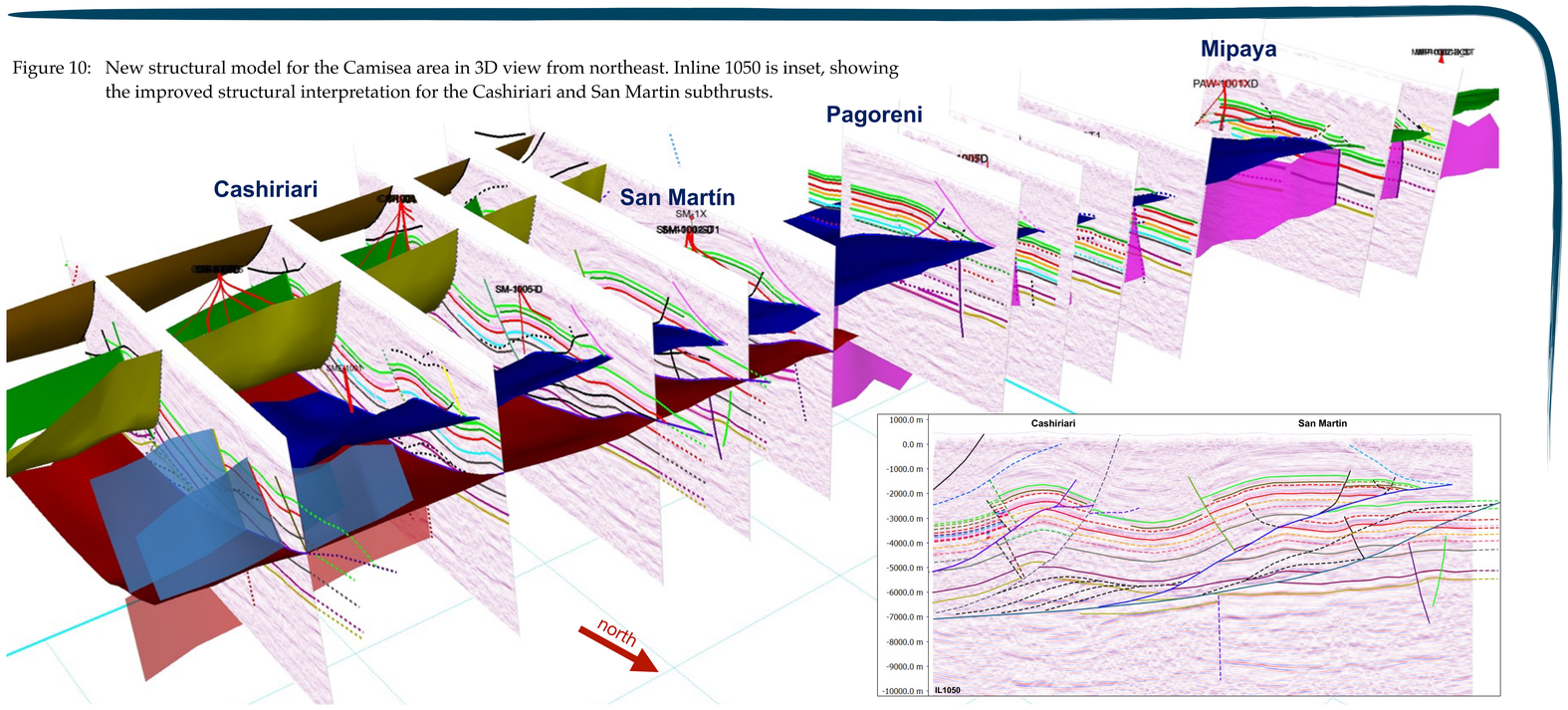

Figure 10: New structural model for the Camisea area in 3D view from northeast. Inline 1050 is inset, showing the improved structural interpretation for the Cashiriari and San Martin subthrusts.

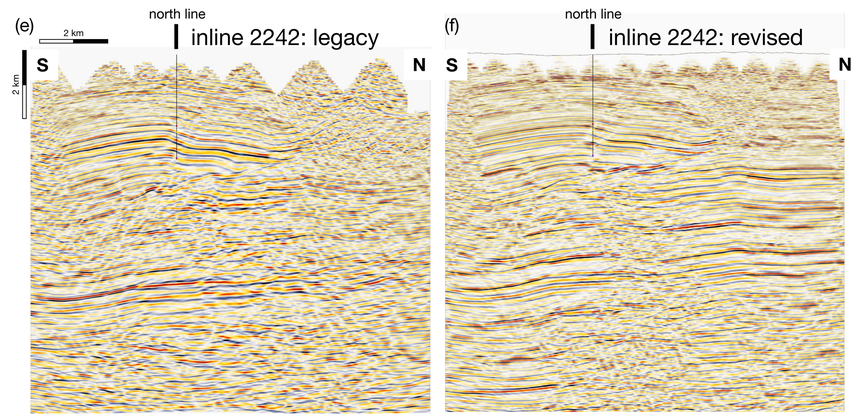

Figure 9: Depth migration results as compared to the legacy processing for three key lines indicated in Figure 3. (a) Legacy version of inline 590, (b) revised version of inline 590. An arbitrary line through the 3D along the northern well locations at 2× vertical exaggeration, (c) legacy and (d) revised versions. Inline 2242 (e) legacy and (f) revised.

Interpretation results

The new interpretation performed on the reprocessed seismic cube showed significant improvements that helped in the structural and stratigraphic interpretation. Among these improvements we have:

- Improvement in the structural image of the Cashiriari and San Martin Sub-Thrusts (Fitzcarrald Sheet) led to new structural model of Camisea area (Figure 10)
- Average absolute value of error in seismic reflector depths is 1.5% (Figure 11)
- Identification of channels and gas-water contact in Vivian reservoir using spectral decomposition (Figure 12)
- Identification of Flat Spot in the Noi reservoir related to gas-water contact
- Potential exploratory areas near the producing fields

Summary and conclusions

Geologic constraints for TTI anisotropic PSDM resulted in the following benefits:

- Velocity structure consistent with the geologic units
- TTI dip model followed structural dip even in areas of low signal
- Consistent velocity structure across low-fold area significantly improved imaging
- Imaged volume tied wells across the block

The seismic-imaging improvements resulted in more accurate mapping of the producing fields and identified potential exploratory areas nearby

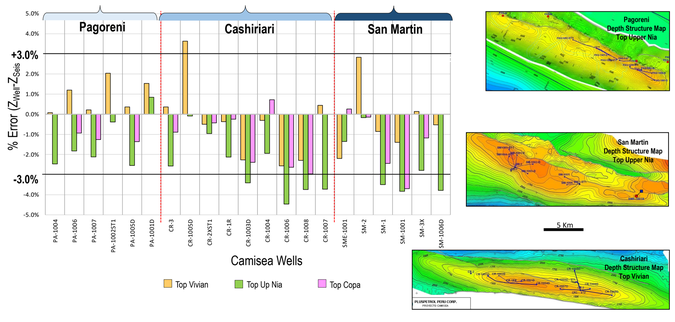

Figure 11: Correlation analysis of well depths to seismic reflector depths. Average absolute value of the percentage error is 1.5%.

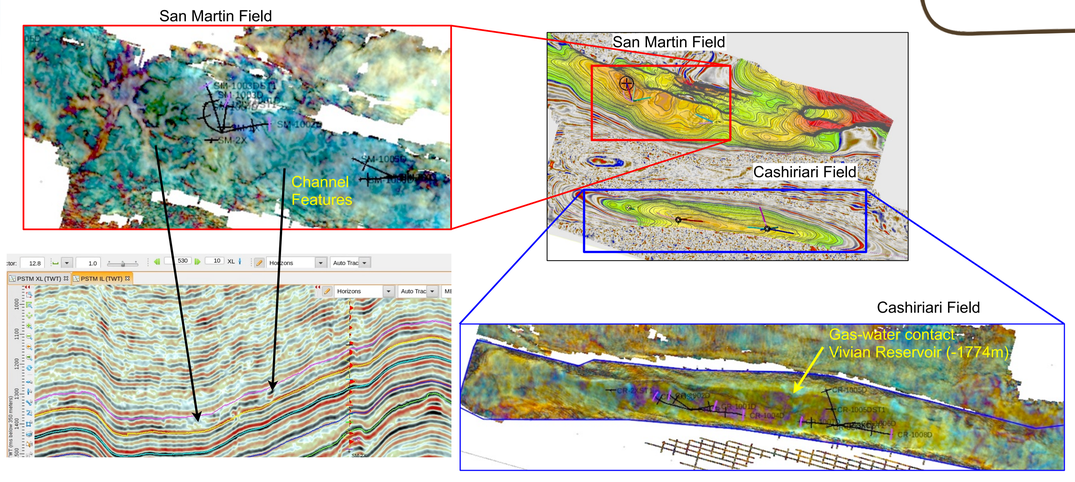

Figure 12: Spectral decomposition: combined frequencies 14Hz, 26Hz, and 38Hz in the Vivian Reservoir

Acknowledgements

The authors wish to thank Pluspetrol and its JV partners for permission to publish these results. We are also grateful Andrew Graham of TBI for optimized migration with Tsunami and the technical support of Raman Singh and openDTect when creating the technical displays.

References

Boyer, S.E., and Elliott, D., 1982. Thrust systems. AAPG Bulletin 66, 1196–1230

DeCelles, P.G., and Giles, K.A., 1996. Foreland basin systems. Basin Res. 8, 105–123

Disalvo, A., Rocha, E., Ching, J.F.C. and Cabré, J.P.D., 2022. The San Martín Anticline: a classic example of a fault-bend fold in the Camisea fold and thrust belt, Central Andes, Perú. In Andean Structural Styles, Elsevier, 285-297.

McClay, K., Scarselli, N., Tamara, J., Hammerstein, J, and Torres, D., 2018, Structural styles of the Camisea fold-and-thrust belt, southeast Peru, in G. Zamora, K. R. McClay, and V. A. Ramos, eds., Petroleum basins and hydrocarbon potential of the Andes of Peru and Bolivia: AAPG Memoir 117, p. 271–296.

Murphy, G. E. & Gray, S.H., 1999, Manual seismic reflection tomography, GEOPHYSICS 64, no. 5, 1546-1552.

Schultz, P., 1998, The Seismic Velocity Model as an Interpretation Asset, Society of Exploration Geophysics.

Vestrum, R.W., Lawton, D.C., and Schmid, R.S., 1999, Imaging structures below dipping TI media: GEOPHYSICS 64, no. 4, 1239-1246.

Vestrum, R.W., and Cameron, G.H., 2022, Seismic imaging in fold-and-thrust belts, In: Andean Structural Styles, A Seismic Atlas, Elsevier, 29–41.

Zamora, G., Louterbach, M. and Arriola, P., 2019. Structural controls along the Peruvian Subandes. In Andean tectonics, Elsevier, 333-362.